

Simulation studies of internal mechanisms in the static deflection of a cellulose electroactive paper actuator

R. P. Joshi^{a)} and F. Mbaye

Department of Electrical and Computer Engineering, Old Dominion University, Norfolk, Virginia 23529, USA

P. Basappa

Department of Electronics Engineering, Norfolk State University, Norfolk, Virginia 23504, USA

S. D. Jang and J. Kim

Department of Mechanical Engineering, Inha University, Incheon 402-751, Korea

J. C. Hall

Department of Chemistry, Norfolk State University, Norfolk, Virginia 23529, USA

(Received 22 August 2007; accepted 10 January 2008; published online 28 March 2008)

Studies of voltage-induced deflections in electroactive paper (EAPap) have been carried out. On the experimental side, measurements of bias-dependent deflections and strain, water absorption as a function of time, and relative humidity were obtained for the cellulose EAPap actuator. In addition, model simulations have also been carried out to probe and quantify the role of the various internal mechanisms responsible for the deflection. Our simulation predictions yield good agreement with the measured deflection data for the EAPap. The modeling suggests that internal ion content and its migration, water absorption leading to a nonuniform permittivity, random variations in the transverse piezoelectric-coupling coefficient $d_{31,i}$, and the modulus of elasticity all collectively contribute to the EAPap deflection electrophysics. It also appears that higher sensitivity, with a minimal bias dependence, could be achieved by deliberately adding ions during EAPap processing.

© 2008 American Institute of Physics. [DOI: [10.1063/1.2891676](https://doi.org/10.1063/1.2891676)]

I. INTRODUCTION

Electroactive polymers (EAPs) exhibit large strain in response to an external electric field and have attracted a great deal of attention in recent years for various applications. These materials include dielectric elastomers, such as acrylics and silicones¹⁻³ and naturally occurring bipolymer cellulose.^{4,5} EAPs have demonstrated large shape changes and actuation strains of up to 380%.^{6,7} No other electric field-activated material comes close to matching such strains. Other favorable properties include soft actuation, ease and simplicity in manufacturing, their light weight, low power consumption, and the ability to withstand harsh environments. Cellulose is the most abundant natural polymer of this type, consisting of glucose-glucose linkages arranged in linear chains^{8,9} and is an inexhaustible source of raw material for environmentally friendly and biocompatible products. Cellulose derivatives are currently used for coatings, laminates, optical films, pharmaceuticals, foods, and textiles. Recently, cellulose has been discovered as a smart material that can be used for sensor and actuator applications.⁹ This material has been termed as electroactive paper (EAPap).

It is projected that EAPs will soon have a great impact in transducer, sensor, and actuator technologies, and will find numerous applications in robotics, prosthetic and artificial muscle-based devices, and microscopic pumps. Space agencies are seeking to reduce the size, power consumption, and cost of instrumentation used in future deep-space

missions.^{10,11} Recent research for NASA applications includes the piezoelectric bending of EAPap sensors under conditions exceeding the harsh environments on Mars. Other space-related applications include motors for antenna and instrument deployment, device positioning, and aperture opening. EAPs have also been termed “artificial muscles” due to their operational similarity to biological muscles.^{12,13}

Wood pulp remains the most important source in cellulose processing. The electromechanical effect in wood was first reported by Bazhenov,¹⁴ while Fukada¹⁵ experimentally obtained the piezoelectric coefficients and demonstrated that oriented cellulose crystallites were responsible for the observed piezoelectricity. EAPap differs from most piezoelectric crystalline materials from the standpoint of its morphological structure. For example, in most sensors and actuators, the EAPap material is processed in the form of a sheet of regenerated cellulose that morphologically has ordered and disordered regions. The ordered domains are mostly crystalline, while the disordered molecules retain preferential direction parallel to the chains in the microfibrils and form surface disorder.⁹ It is conjectured that water molecules would typically be attached to hydroxyl groups within the large disordered cellulose chain regions. Free water would then typically be found in the bulk volume away from the surfaces.

In order to successfully and optimally use cellulose EAP actuators, it is crucial to first understand and quantify the actuation mechanism. Several factors contribute to a more complex situation in EAPap. (i) First, the EAP is noncrystalline with internal heterogeneity and disordered regions. Hence, many of the relevant parameters that contribute to

^{a)}Electronic mail: rjoshi@odu.edu.

piezoelectric bending and produce the dielectric forces are not fixed, but instead vary spatially within the sample. The first demonstration of the role of spatially nonuniform and randomly varying parameters that could lead to substantially larger deflections in biological piezoelectrics was given by Williams.¹⁶ This study arose from the need to adequately explain a previous very surprising result of unusually large deflections observed in disordered polar textures (i.e., tendon and bone segments). The response in that experimental work had shown substantial deviations from the expectations based on crystalline materials.¹⁷ The observed differences led Johnson *et al.*¹⁸ to propose a spatially varying piezoelectric parameter d_{31} . Their model led to deflections in piezoelectric biomaterials that were large and consistent with the experimental observations.

(ii) The second complication arises from the variability in water content within the EAPap. Since EAPap is a piezoelectric material, its deflection will depend on the internal electric field created by the external voltage. This, in turn, is dictated by the permittivity profile. Hence, any process or phenomena that affect the permittivity will influence the deflection and need to be carefully modeled. The EAPap is known to absorb water very easily from the ambient environment.^{19–22} While the relative permittivity of polar water molecules in the unconstrained, continuum state is ~ 81 , this value can dramatically be reduced due to the space confinement effects.²³ The latter is a distinct possibility in the EAPap scenario, due to the attachment of water molecules to the hydroxyl groups within the largely disordered cellulose chains via absorption of the water molecules. Such attachment renders them virtually immobile. The presence of water within EAPap can thus be expected to produce two outcomes: (a) First, the dielectric constant would be spatially nonuniform, with strong localized reductions at the trapping sites. (b) Second, the overall permittivity of the EAPap material would be different from that of the intrinsic polymer alone due to the introduction of water molecules. Thus, Maxwell–Wagner^{24–26} type mixture theories need to be applied to ascertain the effective EAPap permittivity, with superposition of local variability. To the best of our knowledge, such humidity-dependent, spatially nonuniform permittivity models have not been implemented or studied.

(iii) Next, ions are typically known to be present in the EAPap material. This inclusion mainly occurs during processing. Sodium, sulfur, and aluminum are the most abundant. In a recent report,⁹ concentrations of 1693, 2868, and 392 ppm were observed for Na, S, and Al, respectively. The presence of such ions alters the internal electric field and hence affects the piezoelectric forces generated within the EAPap.

(iv) A related aspect is that upon external electric field application, ions within the EAPap can begin migrating. The net effect can be expected to be a dynamic variability in the electric field profile and a delayed polarity dependence of the actuator. A humidity contribution should also result since ionic migration is enhanced in the presence of free water molecules.

In this contribution, we construct a model for the bending deflection of an EAPap actuator. The concepts and physi-

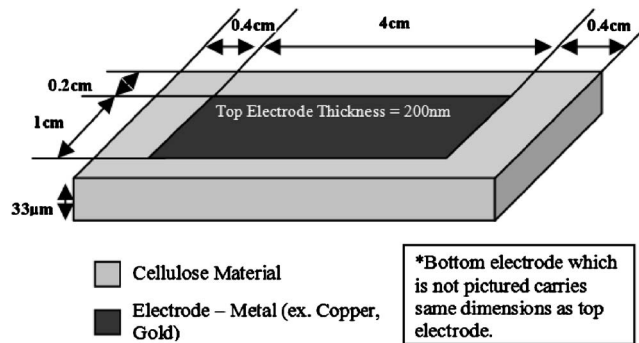


FIG. 1. EAPap geometry.

cal features discussed above have been incorporated to predict the actuator deflections in response to an externally applied dc voltage. The numerical analysis also provides a relative assessment of the contributing factors. Finally, comparisons between the current model predictions and actual experimental data obtained from an actual EAPap bending actuator are presented for model validation.

II. MODEL ANALYSIS

The geometry used in the present calculations consisted of a rectangular EAPap sample with gold plated electrodes on opposite surfaces, as shown in Fig. 1. The flat surface of cellulose sample had dimensions of 4.8 cm (length) by 1.4 cm (width), while the thickness was about 33 μm. The gold electrodes had a length of 4 cm and a width of 1 cm with an approximate thickness of ~ 200 nm. External dc voltage applied to the electrodes created a transverse electric field within the EAPap. The top edge was held fixed producing an effective cantilever type system. For the static analysis of piezoelectric cantilever actuator deflections, we start with the approach employed by Timoshenko²⁷ for a bimorph, two-layer structure, and extended by others.^{28,29} More recent work has utilized electrical equivalent circuits.³⁰ In the present case, the internal heterogeneity is treated by resorting to a multilayer model, with the total thickness L divided into N segments of width dz ($=L/N$). In this model, the material parameters such as the local permittivity, piezoelectric constants, and cross-sectional areas are taken to be constant within a given planar layer, but allowed to vary from one layer to the next. Internal heterogeneity within the EAPap is thus included, though more complex variations, such as islands and clusters within a given layer, could be incorporated as the next level of complexity. For the segmented model, the problem at hand boils down to finding the collective deflection of an N -layer, composite piezoelectric cantilever beam at a given applied voltage.

A method for predicting the static behavior of a piezoelectric cantilever actuator for an arbitrary configuration of elastic and piezoelectric multilayers has been reported by DeVoe and Pisano.³¹ It allows for variations of the elastic and piezoelectric parameters within each constituent segment of an N -layer cantilever beam. The deflection and the overall radius of beam curvature are obtained from the equations of motion for each segment and applying steady state requirements. Though the details are given in Ref. 31, a brief outline

of the piezoelectric multimorph method is as follows. In equilibrium, the sum of the forces F_i and moments M_i within the i th layer must sum to zero. Thus,

$$\sum_{i=1}^{i=N} F_i = 0, \quad (1a)$$

and,

$$\sum_{i=1}^{i=N} M_i = F_1 t_1/2 + F_2(t_1 + t_2/2) + \cdots + F_N \left(\sum_{i=1}^{i=N-1} t_i + t_N/2 \right) = 0. \quad (1b)$$

In the above, t_i is the thickness of the i th layer. The individual moments are related to the radius of curvature r as $r = (\Gamma_i I_i)/M_i$, where Γ_i and I_i are the effective modulus and second moment of inertia, respectively, of the i th layer. Combining Eqs. (1a) and (1b), one gets

$$(1/r) \left[\sum_{i=1}^{i=N} \Gamma_i I_i \right] = F_1 t_1/2 + F_2(t_1 + t_2/2) + \cdots + F_N \left(\sum_{i=1}^{i=N-1} t_i + t_N/2 \right) = 0, \quad (2)$$

which can be cast in the following matrix form:

$$A = \begin{bmatrix} 1/S_1 \Gamma_1 - 1/S_2 \Gamma_2 & 0 & \cdots & 0 & 0 \\ 0 & 1/S_2 \Gamma_2 - 1/S_3 \Gamma_3 & 0 & \cdots & 0 \\ \cdots & 0 & \cdots & \cdots & \cdots \\ 0 & \cdots & 0 & 1/S_{N-1} \Gamma_{N-1} - 1/S_N \Gamma_N & 0 \\ 1 & 1 & \cdots & 1 & 1 \end{bmatrix}, \quad (6a)$$

while B is a column vector containing the various thickness values t_i as

$$B = \begin{bmatrix} t_1 + t_2 \\ t_2 + t_3 \\ \cdots \\ t_{m-1} + t_m \\ 0 \end{bmatrix}, \quad (6b)$$

and the column vector $[C]$ is given as

$$C = \begin{bmatrix} d_{31,1}(E_2 - E_1) \\ d_{31,2}(E_3 - E_2) \\ \cdots \\ d_{31,N-1}(E_N - E_{N-1}) \\ 0 \end{bmatrix}. \quad (6c)$$

$$1/r = \left\{ \left[\sum_{i=1}^{i=N} \Gamma_i I_i \right] \left[t_1/2 + (t_1 + t_2/2) + \cdots \left(\sum_{i=1}^{i=N-1} t_i + t_N/2 \right) \right] \right\} \cdot [F_1 \ F_2 \ \cdots \ F_N]^T, \quad (3a)$$

i.e.,

$$1/r = [D] [F]^T, \quad (3b)$$

where $[F_1 \ F_2 \ \cdots \ F_N]^T$ denotes the transpose of a force vector (i.e., it is a column vector comprised of the various forces F_i), and $[D]$ denotes the row vector containing the Γ_i , I_i , and t_i terms of Eq. (3a). Equating the piezoelectric strains at the interface between the i th and $(i+1)$ th layers results in

$$d_{31,i} E_i + F_i / (S_i \Gamma_i) - t_i / (2r) = d_{31,i+1} E_{i+1} + F_{i+1} / (S_{i+1} \Gamma_{i+1}) + t_{i+1} / (2r) \quad (4)$$

where $d_{31,i}$ is the transverse piezoelectric-coupling coefficient and S_i is the area of the i th layer. This formulation thus allows for internal variability in the material parameters such as $d_{31,i}$, t_i , and S_i . Combining the above equations yields the following final matrix expression involving the radius of curvature r for the composite piezoelectric cantilever beam:

$$[A][F] - [B]/(2r) - [C] = 0, \quad (5)$$

where the matrix $[A]$ is

Solving Eq. (5) yields the radius of curvature and hence the beam deflection δx given as $\delta x = L^2 / (2r)$, where L is the total length of the cantilever beam. The net deflection thus depends on the internal electric field E_i as expressed in vector $[C]$ and needs to be evaluated for each layer self-consistently. For the simpler case of a spatially uniform and constant piezoelectric coefficient d_{31} , the above formulations simplifies down to the more familiar form:³¹

$$\frac{1}{r} = \frac{2d_{31} D A^{-1} C^*}{2 - D A^{-1} B}, \quad (7a)$$

where,

$$C^* = \begin{bmatrix} (E_2 - E_1) \\ (E_3 - E_2) \\ \cdots \\ (E_N - E_{N-1}) \\ 0 \end{bmatrix}. \quad (7b)$$

The applied voltage V across the two opposite sides of the EAPap can be expressed in terms of the electric field $E_i(x)=E(idx)$ within each lateral slice of thickness dx as

$$|V| = \sum_{i=1}^{i=N} \{E_i(x)dx\}. \quad (8)$$

The electric displacement vector $D(=\epsilon E)$ in terms of the permittivity ϵ satisfies the relation

$$S_{i+1}\epsilon_{i+1}E_{i+1} = S_i\epsilon_iE_i + Q_i, \quad (9a)$$

i.e.,

$$E_{i+1} = R_iE_i + T_i, \quad (9b)$$

where Q_i is the charge within the i th segment (possibly due to ions such as sulfur or sodium), $R_i=(S_i\epsilon_i)/(S_{i+1}\epsilon_{i+1})$, and $T_i=Q_i/(S_{i+1}\epsilon_{i+1})$. In general, the permittivity ϵ will be a variable due to the nonuniformities in the water content of each internal segment. For example, absorption from the two surfaces under humid conditions can be expected to increase the water content, and the net permittivity would then be that of a polymer-water mixture. Binding of water molecules within disordered regions of the EAPap can further complicate the permittivity profile, by causing local reductions due to the space confinement effects on water. Coming back to the question of the internal electric field calculations, the cumulative voltage drop across all of the N segments must add to V . Hence, one gets

$$V = \sum_{i=1}^{i=N} E_i t_i = E_1 t_1 + (R_1 E_1 + T_1) t_2 + (R_2 \{R_1 E_1 + T_1\} + T_2) t_3 + \dots + . \quad (10)$$

The electric field profile (i.e., the E_i values) can be fully obtained from Eqn. (10) for given thicknesses t_i , cross-sectional areas S_i , local charge Q_i , and permittivity ϵ_i

The expressions for permittivity to be used for the electric field calculations can be obtained from the Maxwell-Wagner theory²⁴⁻²⁶ of mixtures. According to this theory, the permittivity $\epsilon_{\text{mix}}(x)$ of a mixture at a location x is given by

$$\begin{aligned} \epsilon_{\text{mix}}(x) = & \epsilon_{\text{host}} \{ [2\epsilon_{\text{host}} + \epsilon_{\text{water}}(x)] \\ & - 2p[\epsilon_{\text{host}} - \epsilon_{\text{water}}(x)] \} / \{ [2\epsilon_{\text{host}} + \epsilon_{\text{water}}(x)] \\ & + p[\epsilon_{\text{host}} - \epsilon_{\text{water}}(x)] \}, \end{aligned} \quad (11)$$

where p =volume fraction of water molecules at location x ; Clearly, from Eq. (10), as $p \rightarrow 0$, $\epsilon_{\text{mix}}(x) \rightarrow \epsilon_{\text{host}}$, and as $p \rightarrow 1$, $\epsilon_{\text{mix}}(x) \rightarrow \epsilon_{\text{water}}$. The permittivity of water is roughly $81\epsilon_0$, where the free-space permittivity ϵ_0 equals 8.85×10^{-12} F/m. Typically, the water content within the EAPap is not well characterized and can change dynamically with the ambient humidity. Even for a fixed humidity, the slow absorption of water can lead to a time-varying change in the volume fraction p and hence the local permittivity. Finally, even if the fraction p was known with certainty, the degree of water molecule attachment within the disordered regions of the EAPap is uncertain. Given all of the above difficulties in fixing the internal permittivity, here a number of model spatial profiles will be chosen to predict qualitative trends and

assess the relative impact of water content in EAPap on its piezoelectric deflection.

III. EXPERIMENTAL DETAILS

A. Preparation of cellulose EAPap actuator

Figure 1 shows the cellulose EAPap geometry and configuration as a bending actuator. The fabrication process involved dissolution of the cellulose fiber into solution and making a sheet by using a spin coater. Gold electrodes were deposited on both sides of the cellulose film by means of physical vapor deposition. The thickness of gold electrodes was extremely thin (~ 200 nm), so that their stiffness was negligible compared to that of the host paper. The size of sample was 48×14 mm². Separate measurement confirmed the presence of chlorine ions within the EAPap sample. Though quantitative assessments of the ionic density were not made, their role in affecting the observable strain and deflection can be expected. This aspect is discussed in detail later in the context of the modeling results.

B. Bending displacement measurement

The displacement of the EAPap actuator tip was obtained by using a computerized displacement measurement system, as shown in Fig. 2. The EAPap actuator was supported vertically in an environment chamber that controlled the humidity and temperature. Function generator (Agilent 33220A) controlled by a computer sent the excitation voltage to the actuator and produced a bending deformation. The tip displacement of the EAPap actuator was measured by the high precision laser Doppler vibrometer (LDV), an Ometron VS100, mounted on an optical table and the signal was converted to the displacement through the LABVIEW software in the computer. Simultaneously, the current probe (Tektronix TCPA300) measured the input current supplied from the function generator. The maximum resolution of the LDV was 50 nm.

IV. RESULTS AND DISCUSSION

A. Experimental observations and data

The actual bending displacements of the EAPap actuator obtained as a function of time are shown in Fig. 3 for two different voltage amplitudes. Two aspects are evident from the data. First, the response is roughly linear, with twice the displacements obtained in going from 1 V to the 2 V excitation. Second, a slight time-dependent change in displacement occurs for both amplitudes. The variation is relatively slow and is perhaps indicative of ionic movements inside the sample. This aspect will be discussed in greater detail in the context of the simulation results. Such movements alter the internal electric fields and their gradients, leading to observable changes in the overall actuation forces. As already mentioned, chloride ions were detected in these samples, though their density was not quantitatively measured. Hence, slow changes in the cantilever deflection with time appear quite credible and reasonable.

Next, experimental data on water absorption by the cellulose material in humid environments are shown in Fig. 4.

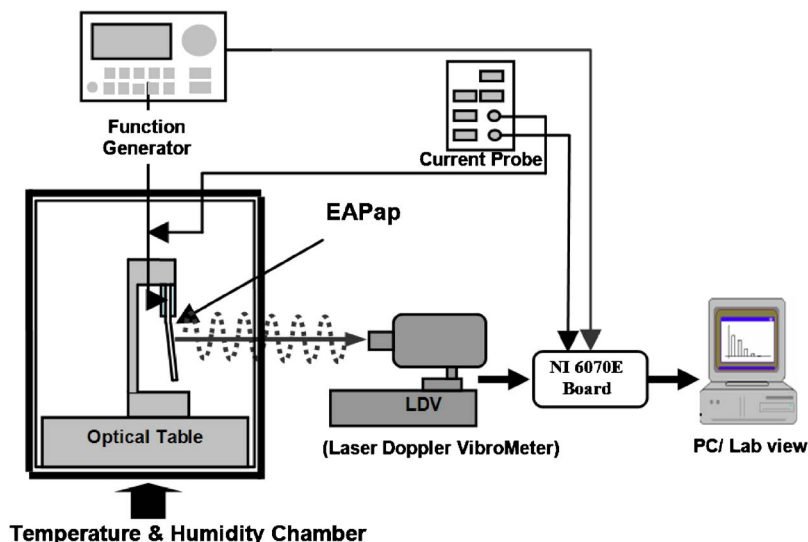


FIG. 2. (Color online) Displacement measurement system.

Three samples were used, and measurements were repeated for each sample to provide more data points. These observations are presented in terms of the weight gain of the EAPap for different values of the relative humidity within the experimental chamber. Each data point represents a steady state condition after which net water absorption by the EAPap ceases. The curve of Fig. 4 is quadratic and indicates that at any finite (nonzero) humidity level, the actuator does contain water molecules within the cellulose matrix. This is an important inference and points to changes in internal polarization due to the contributions associated with the water dipoles. It can also change the internal mobility of ions. Later, in our discussions of the simulation results, this point is revisited.

Finally, measurements of the actuator displacements as a function of the applied bias for a fixed humidity, as well as the deflections for different humidity values for a fixed voltage, were obtained. The results are shown in Figs. 5 and 6,

respectively, for the three samples. The deflection with applied voltage can be fitted to a parabolic curve in Fig. 5, with a slight nonlinearity at higher biasing. Furthermore, the measured displacements were in the 100–400 μm range. The curve of Fig. 6 is less nonlinear, with displacements measured in the 160–230 μm range. The calculations presented in the next section quantitatively examine the displacements at different applied voltages. Various mechanisms and internal processes were invoked in the model calculation. It is shown that general agreement with experimental data and qualitative trends becomes possible only with contribution from internal ions, water dipole, and random spatial fluctuation comprehensively taken into account.

B. Modeling results and discussion

Equal surface areas of each sectional layer in the discretized numerical model lead to zero diagonal elements of

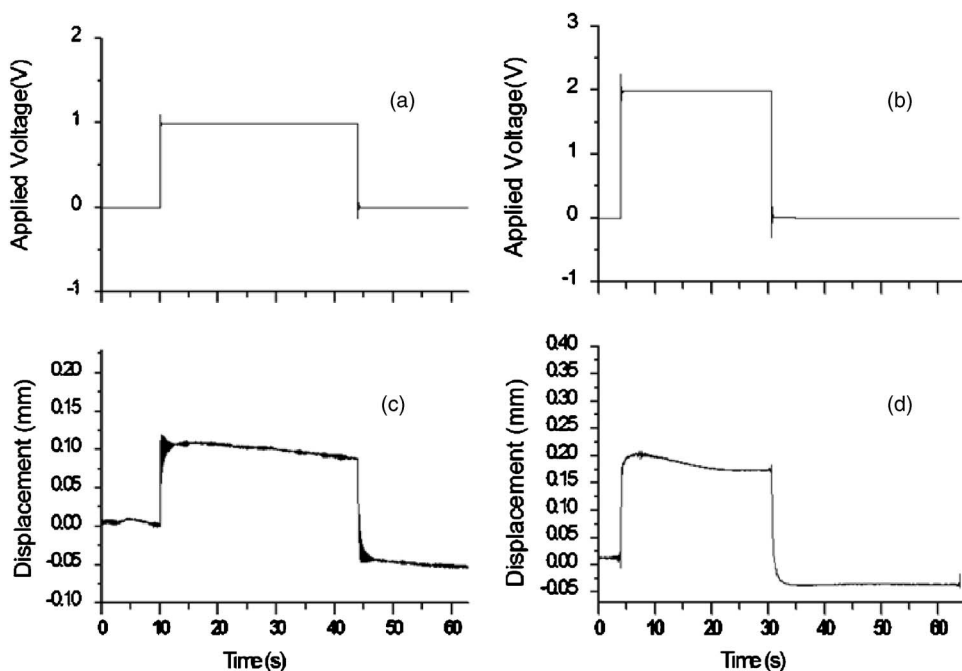


FIG. 3. Waveforms of applied voltage and the corresponding measured displacements. (a) Applied voltage amplitude of 1 V, (b) waveform for 2 V pulse amplitude, (c) time-dependent displacement for the 1 V pulse, and (d) time-dependent displacement for the 2 V excitation.

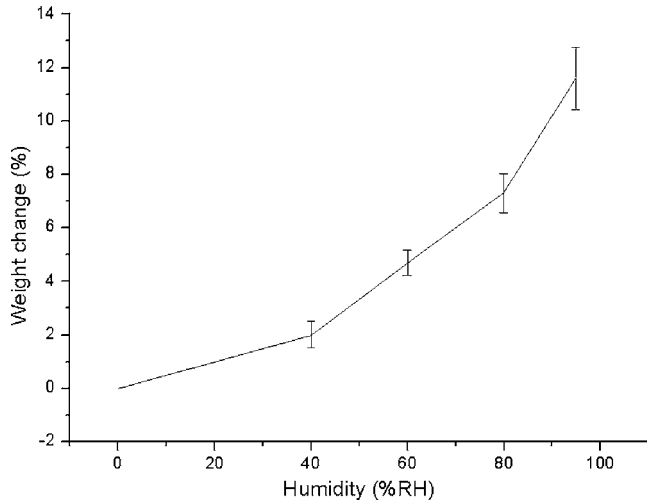


FIG. 4. Relative weight change with varying humidity.

the matrix **A**. The only way of producing a mathematically correct, physical solution is to allow for spatial variations in the modulus parameter. This is reasonable, given the heterogeneity and noncrystalline nature of the material. Hence, a random Gaussian distribution for Γ with a 10 GPa mean value (corresponding to the modulus for Oakwood) and a standard deviation of 1 GPa was assumed.

Simulations were begun by assuming the EAPap to be uniform, with neither water nor ions present and a constant piezoelectric parameter d_{31} . For a $20\epsilon_0$ permittivity, the deflections obtained from simulations with 0–3 V applied biasing were in the 0.6–1.7 μm range. These values are about two orders of magnitude lower than those of the experimental data. In order to refine the model, the permittivity profile was chosen to be spatially variable, as a next step. It was taken to be centrosymmetric and to have a concave-up, parabolic shape with a minimum relative permittivity ($=\epsilon_{r\text{min}}$) of 20. In effect, this amounts to the assumption of water absorption in the EAPap from the two opposite surfaces and its gradual diffusion toward the center. Consequently, regions at the center of the EAPap were taken to remain at the initial “water-free” permittivity value. The results are shown in Fig.

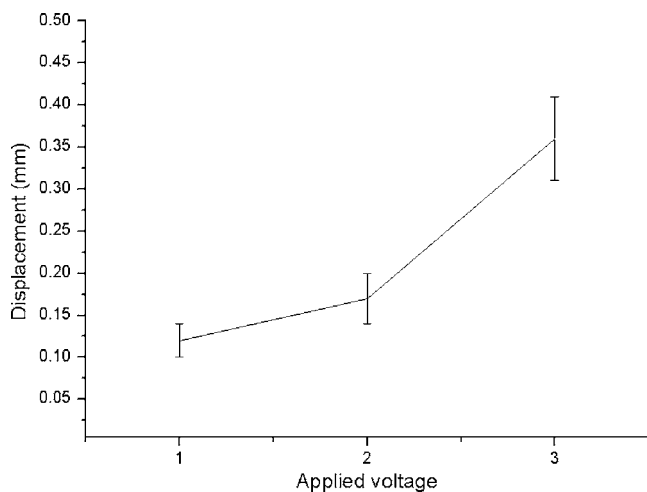


FIG. 5. EAPap actuator displacement as a function of applied voltage at 80% relative humidity.

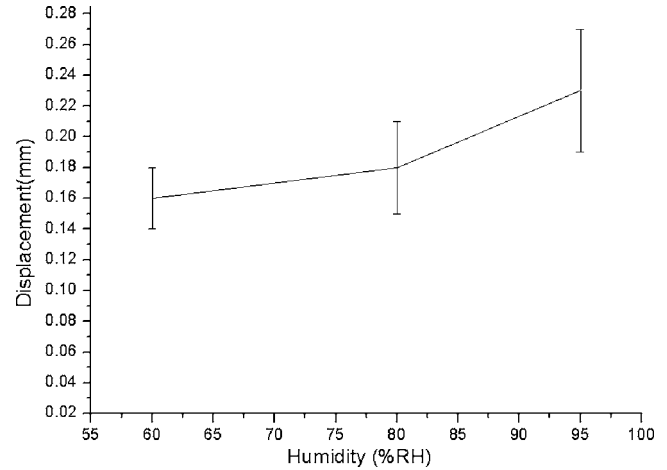
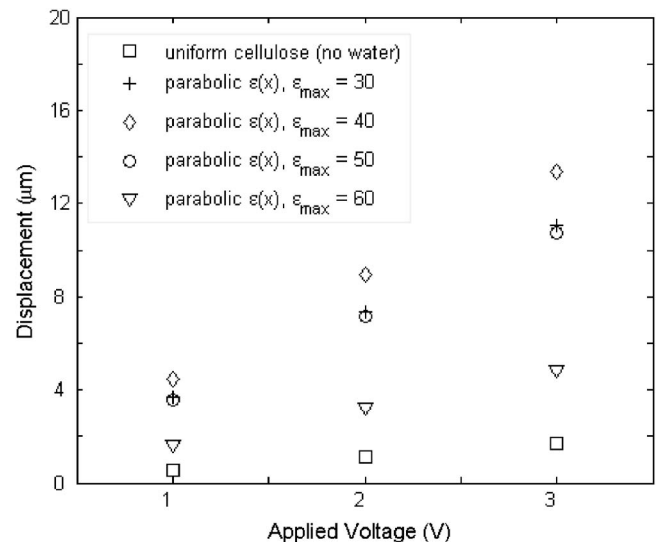
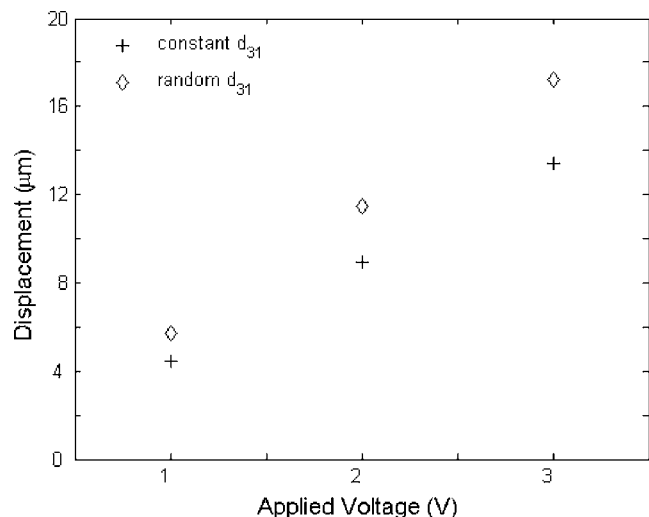


FIG. 6. Displacement vs relative humidity at an applied external bias of 2 V.

7 and deflections increased by almost an order of magnitude. This result underscores the importance of a nonuniform permittivity profile and role for water within the EAPap. However, in Fig. 7 the highest values occur at a relative permittivity of 40 ($=\epsilon_{r\text{max}}$) and subsequently exhibit a decreasing trend for further ϵ_r increases. This aspect does not agree with the experimental results and suggests that further refinements to the model are required.

The above simulation results were obtained using a piezoelectric constant $|d_{31}| = 7 \times 10^{-12}$ m/V. However, one expects the transverse piezoelectric-coupling coefficient to vary throughout the EAPap, due to the inherent heterogeneity. This spatial nonuniformity is associated with the variability of the water content and the molecular composition of the polymer. In order to probe this aspect, simulations were performed again for a parabolic relative permittivity profile with $\epsilon_{\text{max}} = 40$, but with a random d_{31} distribution around a 7×10^{-12} m/V mean and a standard deviation of 1×10^{-12} m/V. This improved the deflection results, as shown in Fig. 8, though close agreement with the available data was still lacking.

FIG. 7. Simulation results with $\epsilon_{r\text{min}}=20$ and different $\epsilon_{r\text{max}}$ values.

FIG. 8. Comparison of deflections between constant and random d_{31} cases.

Next, different ion density profiles were implemented and analyzed to assess their contributions and role in producing EAPap deflections. This affects the electric fields within each layered segment. The simulations discounted any permittivity modifications from water molecules, used a random d_{31} distribution, and yielded the results of Fig. 9. The introduction of ions increased the deflections, bringing the overall predictions closer to experiments. This result confirms the role of ions in contributing to deflections.

Figure 9 shows that the deflection increases with increased ion concentration in the EAPap sample. However, a very high (and perhaps unrealistic) concentration makes the displacement exceed measurements and also leads to a digression from the experimental voltage-dependent trend. For instance, at the ion density $N_i = 10^{20} \text{ cm}^{-3}$ density, the deflections are predicted to be almost independent of the applied bias. This contradicts the experimental voltage dependence

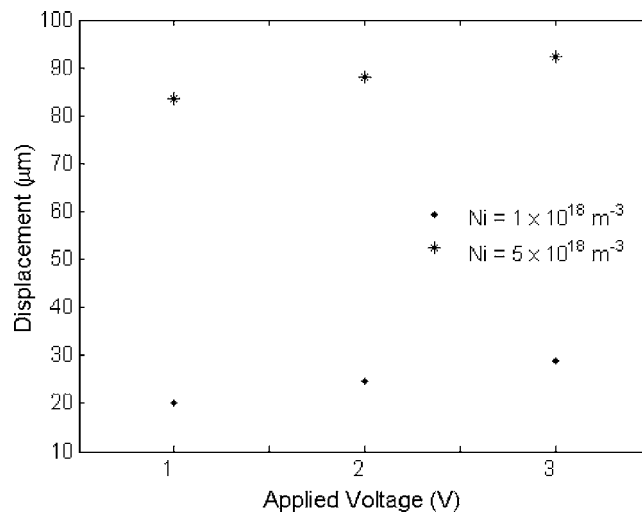
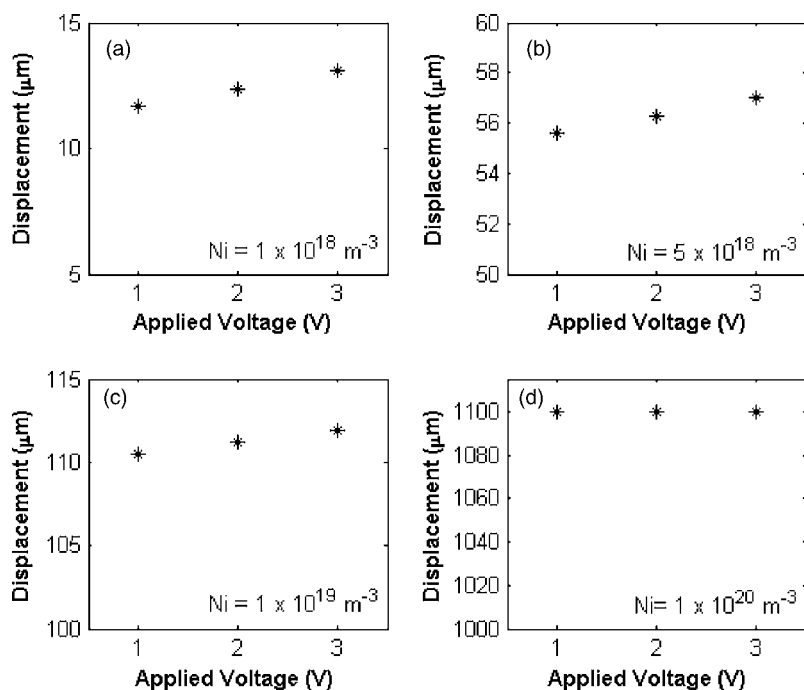


FIG. 10. Displacement results for two different values of uniform ion density in the EAPap sample.

and suggests that the actual samples probably did not contain very large internal ion concentrations. This is indeed true based on the measurements of ionic contents in cellulose EAPap. When the ion contents were determined using inductively coupled plasma mass spectroscopy, the characterization revealed only small amounts of Li^+ ions (84 ppm). As the next progressive step in our modeling study, a parabolic permittivity profile was incorporated next, in addition to internal ions. The results, shown in Fig. 10, reveal an increased overall displacement but the continued absence of strong voltage-dependent deflections.

Given the important role of ions indicated in our simulations, and the inherent nonuniformities within the EAPap material, simulations were next carried out using a *variable ion density* profile. Ionic migration driven by the applied bias forms the physical basis for this spatial ionic variability ar-

FIG. 9. Effect of ion density on the displacement magnitude. A random d_{31} parameter was used.

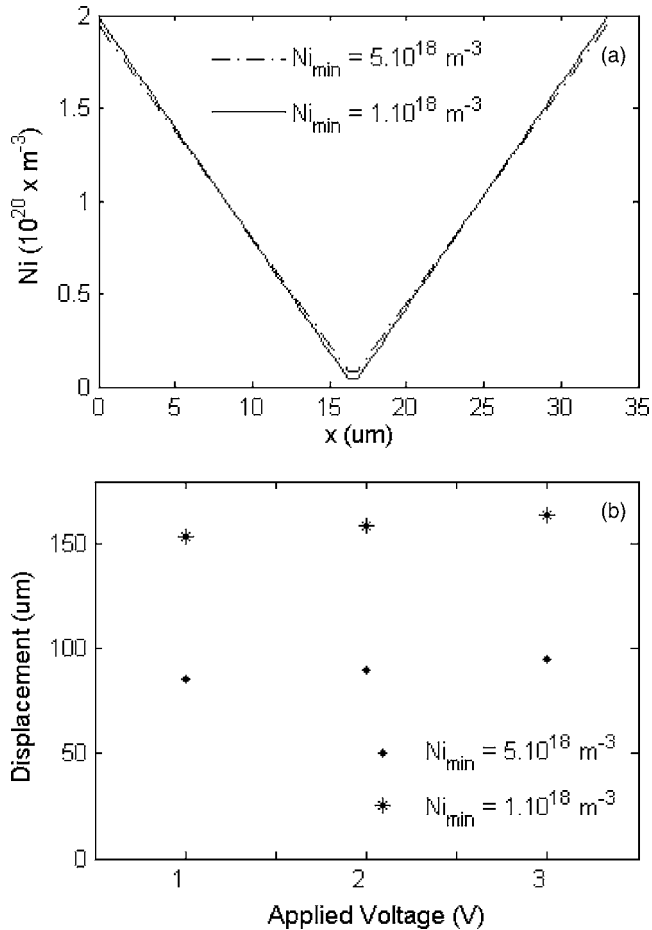


FIG. 11. Simulation with two linear ion density profiles. (a) Ion profiles and (b) corresponding deflection as different applied voltages.

gument. With anions moving to the anode and positive charges toward the cathode, one can reasonably expect more ions to accumulate at the outer surfaces of the EAPap and fewer ions to remain near the center. To zeroth order, this can simply be represented by a linear centrosymmetric profile for the ion density. Numerical simulation results for two different values of $N_{i\text{min}}$ (but a fixed number of total ions within the overall volume) are presented in Fig. 11. The plot shows that as $N_{i\text{min}}$ decreases (i.e., as the linear ion profile curve get steeper) for a fixed number of total ions, the deflection increases as well.

The above result captures both an important physical mechanism and points to an inherent dependence on both duration and magnitude of the external biasing. The latter is in keeping with experimental observations, wherein the deflection was actually seen to change with time (e.g., data of Fig. 3). We also conjecture that entry of water molecules into the EAPap over time further facilitates ion migration. Water absorption by the EAPap over time is corroborated by the dynamic weight changes observed experimentally as in Fig. 4. This hypothesis is also in agreement with measured decrease in deflections of the EAPap with increasing weight, associated with the increased inertia of the sample.

In order to make the spatially nonuniform ion density model more realistic and to have a smooth continuously differentiable profile, the ion distribution was changed from a

TABLE I. Best-fit parameters used.

$N_{i\text{total}}$ (m^{-2})	3.3×10^{15}	3.3×10^{15}	3.3×10^{15}
Bias voltage (V)	1	2	3
$N_{i\text{min}}$ (m^{-3})	1×10^{19}	5×10^{18}	1×10^{15}
ϵ_{max}	60	65	65
ϵ_{min}	20	20	35
Deflection (mm)	0.122	0.185	0.33

linear to a parabolic, concave-up, centrosymmetric shape. Simulations were performed to include parabolic permittivity variations, and the parameter values varied for best-fit deflections with applied bias. Table I lists the resulting values. The voltage-dependent deflections are given in Fig. 12. For a 1 V applied bias, the ions can be expected to start migrating toward the edges and the permittivity can be assumed to attain a rough parabolic profile due to the water absorption. It may be recalled that experimental values were obtained under 80% humidity conditions, and so water absorption must occur. With a 2 V applied bias, with the sample still within the humid chamber, the EAPap would continue to absorb water strongly. Hence, the permittivity at the edges would increase, and further ion migration would be expected to translate into a decrease in $N_{i\text{min}}$. Accordingly, a lower $N_{i\text{min}}$ value (as was used in Table I) seems appropriate for simulations with increasing bias. With a 3 V bias subsequently applied to the same sample, water saturation at the edges of the EAPap could reasonably be expected. Thereafter, the relative permittivity ϵ_{max} at the edges would not be expected to increase any further, but ϵ_{min} at the center should get augmented. The values of Table I were chosen on this qualitative basis and seen to lead to satisfactory agreement with measured data. It may be mentioned that the 3 V case shows a slightly greater error margin. This might be due to other factors not taken into consideration, such as nonlinear material response, anisotropy of the piezoelectric parameter, and random fluctuations superimposed on the parabolic profiles used here.

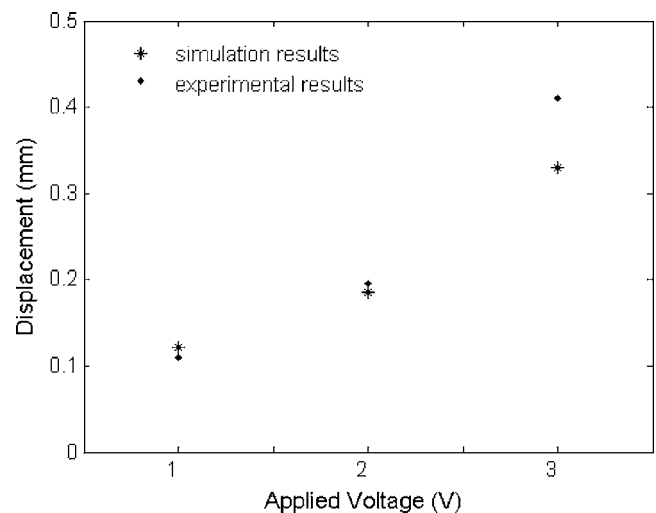


FIG. 12. Results of comprehensive simulations with parabolic ion profile and best-fit parameters. Measured data are also shown.

V. CONCLUDING SUMMARY

Studies of voltage-induced deflections in EAPap were carried out. Experiments were indicative of the hygroscopic nature of the cellulose material, and voltage-dependent deflections were measured. Model simulations were also carried out to probe the role of the various internal mechanisms and provide insights into the deflection electrophysics. The theoretical treatment, based on a layered model for EAPap, included a comprehensive treatment of ionic content, its spatial variations, changes in permittivity, and the random profile for the piezoelectric parameter. Our simulations yielded a good agreement between the predicted EAPap deflections and the measured data. In summary, internal ion content and its migration leading to internal spatial variability and a time-dependent behavior, water absorption leading to a nonuniform permittivity, random variations in the transverse piezoelectric-coupling coefficient $d_{31,i}$, and the modulus of elasticity were all shown to contribute toward determining the final deflection of the EAPap. The calculations also suggest that higher sensitivity, with a minimal bias dependence, could be achieved by adding ions during EAPap processing.

ACKNOWLEDGMENTS

Useful discussions with K. Song (Norfolk State University), A. Pisano (University California, Berkley) and Y. Bar-Cohen (JPL, Caltech.) are gratefully acknowledged. The experimental work was supported by the Creative Research Initiation (EAPap Actuator) of KOSEF/MOST. Support from the Center for Biotechnology and Biomedical Sciences at Norfolk State University under NIH Grant No. P20 MD001822-02 is gratefully acknowledged.

¹D. Klemm, *Comprehensive Cellulose Chemistry* (Weinheim, New York, 1998).

²E. Fukuda, *J. Phys. Soc. Jpn.* **10**, 149 (1955).

³F. F. Kollman and W. A. Cote, *Principles of Wood Science and Technology* (Springer-Verlag, New York, 1968).

⁴C. H. Je and K. J. Kim, *Sens. Actuators, A* **112**, 107 (2004).

⁵J. Kim, J. Y. Kim, and S. J. Choe, *Proceedings of the SPIE's Seventh Annual Symposium on Smart Structure and Materials, Newport Beach, CA*, 2000 (unpublished), pp. 203–209.

⁶R. E. Pelrine, R. D. Kornbluh, and J. P. Joseph, *Sens. Actuators, A* **64**, 77 (1998).

⁷Y. Bar-Cohen, *Proceedings of SPIE Conference on Structures, Structural Dynamics and Materials*, 2001 (unpublished), Vol. 4, pp. 2313–2321.

⁸J. Kadla and R. Gilbert, *Cellul. Chem. Technol.* **34**, 197 (2000).

⁹J. Kim, S. Yun, and Z. Ounaies, *Macromolecules* **39**, 4202 (2006).

¹⁰X. Bao, Y. Bar-Cohen, Z. Chang, and S. Sherrit, *Proceedings of the SPIE-The International Society for Optical Engineering*, 2003 (unpublished), Vol. 5051, pp. 381–388.

¹¹Y. Bar-Cohen, S. Sherrit, X. Bao, and Z. Chang, *Proceedings of the SPIE-The International Society for Optical Engineering*, 2002 (unpublished), Vol. 4946, pp. 8–16.

¹²Y. Bar-Cohen, *Progress in Biomedical Optics and Imaging-Proceedings of SPIE*, 2005 (unpublished), Vol. 5720, pp. xxxiv–xl.

¹³J. W. Paquette and K. J. Kim, *Int. J. Solids Struct.* **29**, 729 (2004).

¹⁴V. A. Bazhenov, *Piezoelectric Properties of Woods* (Consultants, New York, 1961).

¹⁵E. Fukada, *IEEE Trans. Ultrason. Ferroelectr. Freq. Control* **47**, 1277 (2000).

¹⁶W. S. Williams, *Ferroelectrics* **41**, 225 (1982).

¹⁷W. S. Williams and L. Breger, *J. Am. Ceram. Soc.* **58**, 415 (1975).

¹⁸M. V. Johnson, W. S. Williams, and D. Gross, *J. Biomech.* **13**, 565 (1980).

¹⁹S. Boutros and A. A. Hanna, *J. Polym. Sci., Polym. Chem. Ed.* **16**, 89 (1978).

²⁰A. J. Stamm, *Wood and Cellulose Science* (Ronald, New York, 1964).

²¹J. Tsutsumi and H. Watanabe, *J. Jpn. Wood Res. Soc.* **11**, 232 (1965).

²²T. F. Otero, I. Cantero, and S. Villanueva, *Proceedings of the SPIE-The International Society for Optical Engineering*, 1999 (unpublished), Vol. 3669, pp. 26–34.

²³V. Ballenegger and J. P. Hansen, *J. Chem. Phys.* **122**, 114711 (2005).

²⁴J. C. Maxwell, *A Treatise of Electricity and Magnetism* (Dover, New York, 1954).

²⁵K. W. Wagner, *Arch. Elektrotech. (Berlin)* **2**, 371 (1914).

²⁶H. Fricke, *J. Phys. Chem.* **57**, 934 (1953).

²⁷S. Timoshenko, *J. Opt. Soc. Am.* **11**, 233 (1925).

²⁸J. G. Smits and W. S. Choi, *IEEE Trans. Ultrason. Ferroelectr. Freq. Control* **38**, 256 (1991).

²⁹C. Huang, Y. Y. Lin, and T. A. Tang, *J. Micromech. Microeng.* **14**, 530 (2004).

³⁰J. Ajitsaria, S. Y. Choe, D. Shen, and D. J. Kim, *Smart Mater. Struct.* **16**, 447 (2007).

³¹D. L. DeVoe and A. P. Pisano, *J. Microelectromech. Syst.* **6**, 266 (1997).